

Prediction of relative permeability and fast wettability assessment using Digital Rock Physics: An operational study on a Reservoir Sandstone

Mohamed Regaieg^{1*}, Tityl Farhana Faisal¹, Franck Nono², Fabrice Pairoys¹, Victor Fernandes¹ and Cyril Caubit¹

¹TotalEnergies OneTech, Pau France

²Akkodis

Abstract. With the anticipated decline in oil demand over the coming decades, fast appraisal of oil fields becomes crucial for energy companies. In this regard, accelerating petrophysical synthesis plays a significant role in fast appraisal and development of oil fields. Digital Rock Physics (DRP) simulation offers a cost-effective and rapid approach to compute relative permeability curves for rock/fluid systems. It also presents an opportunity to provide reservoir engineers with additional data, thereby enhancing the quality of petrophysical input for their simulations. Previous research demonstrated the predictive capabilities of DRP simulation coupled with a wettability anchoring experiment for a mixed-wet Bentheimer formation [1]. In this study, we applied TotalEnergies' DRP simulation workflow, coupled with a wettability anchoring experiment, in an operational context on a Reservoir sandstone sample. The study was conducted as a blind test prior to the SCAL (Special Core Analysis) measurements. Initial images representing large volumes with low resolution were enhanced using Enhanced Super Resolution Generative Adversarial Networks (ESRGAN) to obtain high-resolution images. Subsequently, a pore network was extracted, and a parallel pore network simulator was utilized for multiphase flow simulations, incorporating the constraints derived from the anchoring experiment to minimize uncertainty. The obtained results were then compared against an in-house SCAL experiment to assess the predictive power of our DRP workflow and the accuracy of the wettability anchoring experiment. Furthermore, new simulations were conducted on a different facies using a new sample without the need for a new anchoring experiment. Finally, the extrapolated simulation results were compared to an in-house SCAL experiment, allowing for an evaluation of the extrapolation capabilities of DRP simulation.

1 Introduction

Over the past 25 years, Digital Rock Physics (DRP) has emerged as a highly enticing technology within the oil and gas industry. Its potential to accurately predict petrophysical properties of Reservoir rocks numerically without the need for extensive SCAL experiments, has captured the attention and interest of energy companies. However, the actual implementation of DRP has proven more challenging than initially anticipated. Two major limitations have been identified: the constraint on image resolution [2] and the characterization of rock/fluids wettability [3,4].

One criticism directed towards DRP is its limitation to compute properties based on relatively small rock volumes, without providing sufficient evidence that the Representative Elementary Volume (REV) for single phase and two-phase flow has been reached. Additionally, concerns have been raised regarding the potential dominance of finite size and boundary effects in the simulations. To address these limitations, our previous work [5] employed the ESRGAN method to enhance image resolution, resulting in larger images with improved clarity. Moreover, we developed a stitching algorithm to extract pore networks from these enlarged images.

We have also focused on advancing our capabilities for large-scale simulations by parallelizing our in-house pore scale simulator [6,7]. By harnessing the power of parallel computing, we overcame the computational challenges associated with simulating large rock volumes accurately. The characterization of wettability plays a crucial role in DRP simulation, as it governs the capillary forces and, consequently, the order of invasion. However, it is a challenging task to accurately characterize wettability, especially in scenarios involving mixed-wet conditions. In such cases, it becomes important to determine the fraction of oil-wet (OW) and water-wet (WW) pores, as well as the spatial distribution of oil-wet pores and their correlation with pore radii. These parameters need to be appropriately incorporated into the model to avoid excessive degrees of freedom and enhance the accuracy of predictions.

Sorbie and Skauge [3] emphasized that wettability assignment is the most complex and least validated stage in the DRP simulation workflow. Similarly, Bondino et al. [4] concluded that achieving "genuine prediction" of multi-phase flow properties hinges upon significant advancements in the characterization of wettability at the pore scale.

Recent developments have made contact angle measurements from micro-CT images of multiphase flow experiments

* Corresponding author: mohamed.regaieg@totalenergies.com

highly appealing [8]. However, these measurements rely on the computation of the three-phase contact line, making them sensitive to image resolution. Insufficient resolution can lead to contact angle values close to 90 degrees, accompanied by large standard deviations [9]. Moreover, automated contact angle measurements account for the presence of pinned menisci, which differ from the contact angle input required by a PNM simulator.

Recent observations [10,11] have indicated spatial correlation of wettability, with pores of similar wettabilities tending to be located in close proximity. However, verifying the existence of this correlation and measuring the correlation length for a specific system is not a straightforward task. It necessitates conducting multiphase flow experiments and ensuring the presence of multiple menisci in neighboring pores, which is not always feasible. Additionally, quantifying the correlation length requires intensive image processing, which is not ideal for an industrial workflow [11].

In order to address these challenges, we have created an innovated DRP simulation anchoring [1,7], which offers a rapid and straightforward implementation within an industrial workflow. This experiment provides valuable insights into the wettability of a sample. Through our analysis, we are able to quantify the proportions of oil-wet (OW) and water-wet (WW) pores, establish correlation between wettability and pore radius, and even estimate the correlation length of wettability if there is spatial correlation present. This innovative approach offers an efficient solution to overcome these limitations. This experiment also provides some measurements such as the endpoints of the relative permeability curves that help constrain the DRP simulations and reduce the uncertainty further.

In this paper, we present an operational study where our Digital Rock Physics technology has been used to predict relative permeability and provide a fast wettability measurement on a Reservoir Sandstone rock that we name Reservoir Rock C.

Initially, we employ ESRGAN to enhance the resolution of our images. This enables us to obtain high-quality images that accurately capture intricate details, even when dealing with larger volumes.

Subsequently, Generalized Network Modelling (GNM) [12] technique is used to extract a pore network with conductivities computed using Direct Numerical Simulation (DNS) on the rock image. Several pore networks are then assembled using an in-house stitching methodology [5]

A wettability anchoring experiment was performed on this sample and allows us to find the wettability input of the simulation as well as performing some measurements that are used to constrain our model further.

Large simulations are performed using TotalEnergies parallel in-house PNM simulator. These simulations are performed using a statistical uncertainty approach that is used to vary the uncertain simulation parameters and only keep the realizations in agreement with the wettability anchoring experiment results. Hundreds of different realizations are used to produce P10, P50 and P90 (scenarios defined in Section 5) relative permeability sets.

In order to validate the approach, simulated relative permeability curves are compared in a blind test to an in-house SCAL experiment performed on the same sample/fluids to assess the predictive potential of our simulation workflow.

Once the simulation validated, the simulation workflow is applied (without repeating the wettability anchoring experiment) on a new sample from another facies. Then, the results are compared to a second SCAL experiment performed on the new sample.

2 Higher resolution images using Enhanced Super Resolution Generative Adversarial Network (ESRGAN)

The initial step in DRP simulation involves the acquisition of micro-CT images of a rock. Subsequently, these images are segmented to differentiate the rock from the pore space. The final stage entails conducting flow simulations to calculate advanced rock properties like relative permeability and capillary pressure. Research conducted by [13] has demonstrated that well-characterized pore space geometry leads to good performance of flow simulators.

Nevertheless, the geometry of actual rocks is not always adequately characterized, primarily due to limited image resolution. This limitation introduces uncertainties in the pore and throat geometry, thereby generating errors in the computation of rock properties. Additionally, compromises are often made during image acquisition regarding the trade-off between acquisition speed, scanned volume size, and obtained resolution. Typically, increasing the resolution reduces the field of view, thus limiting the amount of information extracted from the image. Consequently, this compromises the representativeness of DRP simulations.

In order to solve these issues, we have implemented ESRGAN method [14] with some adjustment to adapt it to micro-CT images (check [5] for more details).

We have made the training parallel using multiple nodes and multiple GPUs in each node. The training is performed using two scans of the same small volume (1.34 microns image and 5.36 microns image), 3000 crops of 384*384 pixels images are made to form the training dataset.

We divided the dataset into training and test datasets. After the training and the resampling of the low-resolution dataset in the Z direction, the generator is applied on 2D slices of 1172*1290 pixels to generate a 3D image of 4688*5160*4800 voxels. The testing was performed on a sub-volume of this image.

Fig 1 showcases the results obtained through ESRGAN, demonstrating high perceptual quality that effectively captures intricate rock textures and previously unresolved clay features in the low-resolution image. The ESRGAN outputs exhibit a striking resemblance to their high-resolution counterparts. It is important to note, however, that this study does not evaluate or report conventional image-based metrics such as Peak Signal to Noise Ratio (PSNR) and Structural Similarity Index (SSIM). Such metrics can be misleading when applied to micro-CT images trained using independent acquisitions and may not be the most suitable indicators for the specific context at hand. Consequently, we also chose to evaluate our results by comparing relevant petrophysical properties. In order to achieve this, we performed single and multiphase flow DRP simulations using the exact same image volumes of high-resolution, low-resolution, and ESRGAN-enhanced images.

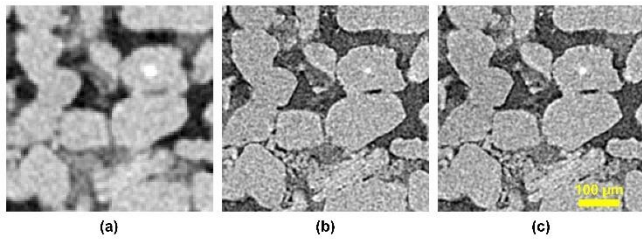


Fig 1 : Comparison between low resolution (5.36 microns) (a), high resolution (1.34 microns) (b) and super resolution (1.34 microns) (c) cropped images of Reservoir Rock C with a factor 4 resolution enhancement on the test dataset

In our image segmentation approach, we utilized the Trainable WEKA Segmentation method [15], which employs the Random Forest (RF) machine learning algorithm. Previous research [16] demonstrated that, when properly trained, Trainable WEKA Segmentation outperformed seven other image-processing pipelines without the need for prior filtering. Moreover, a benchmark study conducted by Reinhardt et al [17] revealed that RF-based approaches minimized user bias compared to other machine learning and conventional segmentation techniques, thanks to continuous interaction between experienced users and the RF classifier.

However, it should be noted that high classification uncertainty may arise in areas with phase transition voxels and tight pore connections due to the partial volume effect. This uncertainty can introduce increased user bias, as highlighted by [17]. To address this, we performed three realistic segmentations that mimic the choices made by experienced users. The "base" case represents the ideal segmentation with high confidence, which would be chosen if only a single segmentation were performed for each image. From this base case, we derived two additional cases, "min" (lower porosity than the base case) and "max" (higher porosity than the base case), by focusing on the pore-grain transition voxels, as depicted in **Fig 2**. This approach allowed us to evaluate a range of feasible segmentation results instead of relying solely on a single solution. It further emphasized the increased susceptibility of low-resolution (LR) images to user bias for the same given volumes.

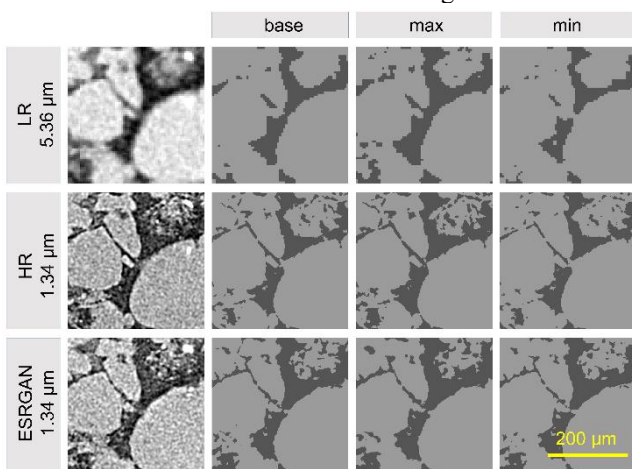


Fig 2 : Example of the several segmentation hypotheses considered in this work for low-resolution (LR), high resolution (HR) and super-resolution (ESRGAN) with factor 4 resolution enhancement on Reservoir C image.

After segmenting the images, we proceeded to compare the porosity and absolute permeability of the test subset using computations performed with OpenFOAM. In **Fig 3**, it can be observed that the enhanced resolution of ESRGAN images reduced segmentation uncertainty, resulting in lower dispersion in the porosity and permeability results. While the base segmentations of the low-resolution images did not consistently yield poor results, we noted that different users may have segmented the images differently, particularly due to the large uncertainty range in porosity and permeability estimations for low-resolution images.

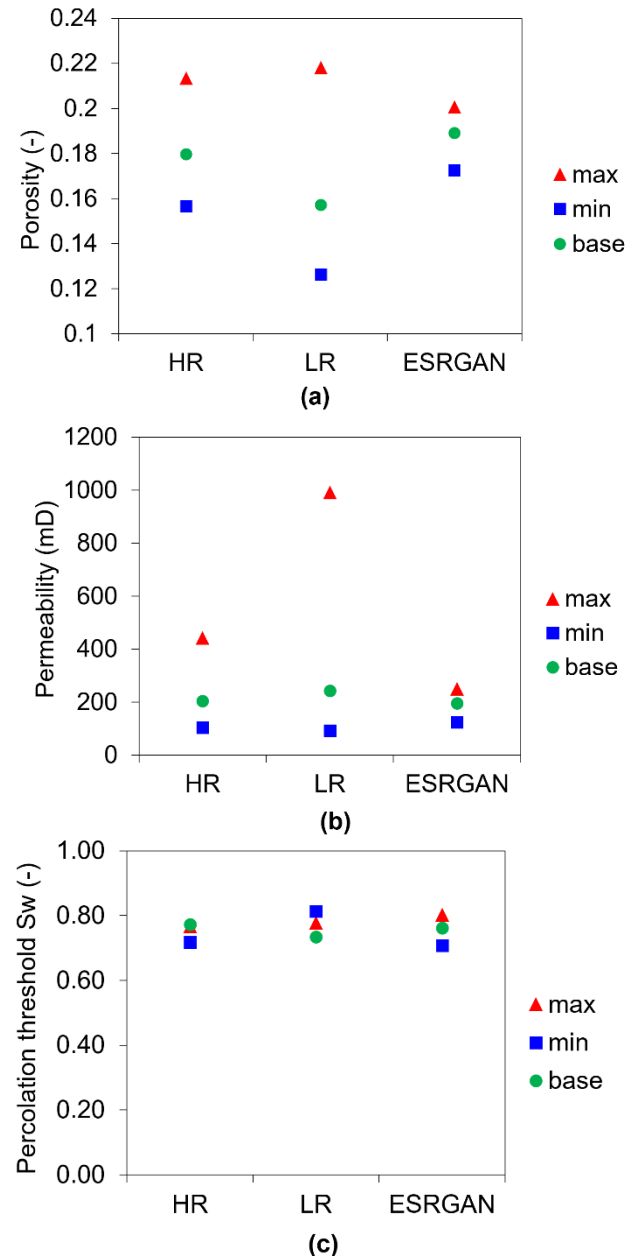


Fig 3 : Porosity (a), permeability (b) and percolation threshold (c) evolution depending on image resolution and segmentation hypothesis on Reservoir C images for factor 4 enhancement

Following the validation of our method on single-phase properties, we proceeded to verify whether ESRGAN-generated images produced comparable results to high-resolution images of the same volume in terms of multiphase flow behavior. To achieve this, we conducted multiphase flow simulations utilizing our DRP simulation workflow, which is based on a pore network modeling technique described by [6,7,18].

In Fig 4, we present the simulated primary drainage capillary pressure curves obtained using low-resolution, high-resolution, and super-resolution images for Reservoir C. As mentioned earlier, we performed several realistic segmentations for each case to illustrate the associated uncertainty, resulting in the presentation of capillary pressure curve envelopes. It is evident from the figure below that the utilization of ESRGAN improves the accuracy of our simulated primary drainage capillary pressure curves.

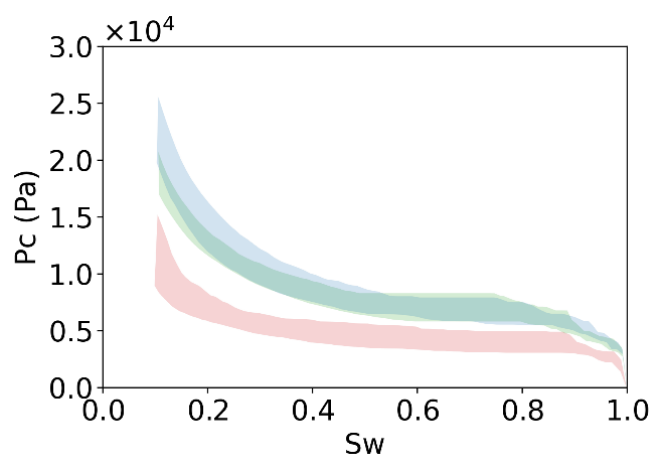


Fig 4 :Comparison between computed capillary pressure curves using 3 images with several realistic segmentation: low resolution (red), super resolution (blue) and high resolution (green)

Following the testing of the model, we perform inference on 5.36 microns images and we generate 3 datasets representing each a cube of 5000^3 voxels that are used in the pore network simulations.

3 Pore Network Extraction

In contrast to certain digital rock physics methods, pore network models do not involve conducting two-phase direct flow simulations within a 3D digital rock. Instead, they rely on extracting a pore network from 3D reconstructions. Various algorithms are available to extract the skeleton of the 3D model, which contains essential geometric and topological information about the underlying pore system. In this study, we utilize a pore network extraction platform called GNextract, developed in collaboration with Imperial College London [12].

GNextract is employed to reconstruct an upscaled version of the 3D segmented image of a rock, generating a network composed of pore elements. The single-phase flow conductances within each pore are determined by solving the

Stokes equation within the original geometry using OpenFOAM. However, it should be noted that the extraction code requires a significant amount of memory to process large images (more than 60 GB of RAM for a 1500^3 voxels image). To overcome this limitation, a stitching process has been developed (more details can be found in [5]). This involves extracting networks from overlapping sub-volumes of the given image and subsequently combining them to reconstruct the complete pore network. With this methodology, 3 pore networks have been extracted from the super resolution images and each had around 8 million pore elements.

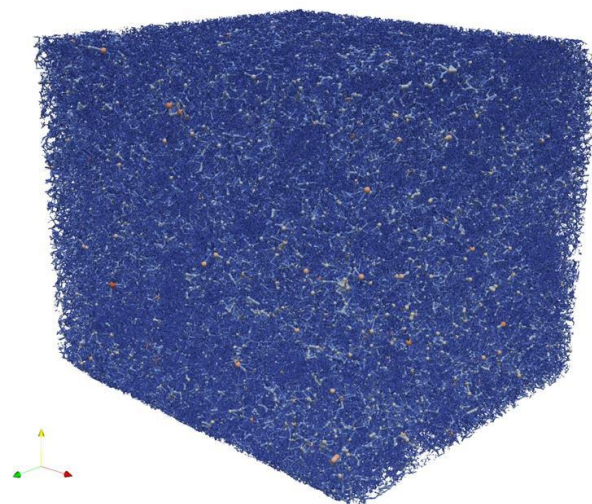


Fig 5 : Large pore network extracted from $5000 \times 5000 \times 5000$ voxels image

4 Wettability anchoring experiment

The role of wettability is of utmost importance in pore network modeling (PNM) simulations, however, accurately characterizing it in advance poses a significant challenge. Even when attempting a qualitative assessment of wettability, such as categorizing it as water-wet, oil-wet, or mixed-wet, numerous uncertain parameters persist, particularly in the case of mixed-wet scenarios. These parameters encompass contact angles, fractions of oil-wet and water-wet pores, spatial correlation of wettability, and correlation of wettability radii. Each of these parameters can exert a substantial influence on simulation outcomes, introducing considerable uncertainties when considering the entire range of potential values for these inputs.

Conducting traditional wettability tests, such as the Amott Harvey or USBM methods, is time-consuming and may not provide all the necessary information required for accurate simulations. To address these challenges and reduce uncertainty, we have developed a fast wettability anchoring experiment utilizing micro-CT imaging. This experiment provides crucial data for the wettability inputs in our simulations, along with measurements that help constrain the simulation and reduce uncertainty. It also provides a much faster wettability characterization experiment comparing to the classical methods [1]. In a previous work, we applied this

approach to a Bentheimer sample [7] and the details of this experimental setup and results will be described in the following section. The goal is to leverage this fast wettability anchoring experiment to obtain essential information for input parameters and improve the reliability and accuracy of our PNM simulations.

The experiment starts by installing a Reservoir C sample with a diameter of 10 mm into a flow cell under a confining pressure of 50 Bars, as illustrated in Fig 6. The initial step involves achieving the initial water saturation (S_{wi}) viscous displacement with mineral oil (Marcol52). The experimental conditions, including capillary number and choice of fluids, remain consistent with the validation SCAL experiment outlined in the subsequent section.

Once S_{wi} has been established, 5 pore volumes (PVs) of toluene are injected to replace the mineral oil, followed by 5 PVs of the reservoir dead crude oil. The sample is then subjected to a four-week dynamic aging process at 90°C, following a similar protocol as the SCAL experiment : injection of 10 PVs of crude oil at a very low capillary number. After aging, the dead crude oil relative permeability ($K_{ro} @ S_{wi}$) is measured, revealing no decrease during aging.

Without the possibility of conducting the entire experiment in the micro-CT under high temperature, we had to return to ambient temperature for the acquisition of 3D X-ray images. To prevent the wax formation from the crude oil, we had to replace it with a mineral oil (M52) before reducing the temperature. To do so, 2.5 pore volumes of decalin are injected to minimize any alteration in the plug's wettability while avoiding a direct contact between the dead crude and the mineral oil. Subsequently, 10 pore volumes of mineral oil (Marcol52) are introduced to replace the decalin. Notably, the fluid replacement process is carried out at low flow rates to minimize any changes in the initial water saturation after ageing.

Once the temperature is reduced and the replacement is completed, an image acquisition step is carried out. Subsequently, a spontaneous imbibition phase is initiated using a one-end-opened protocol. In this process, water spontaneously infiltrates the sample from the bottom face while oil is expelled from the same side, establishing a counter-current imbibition phenomenon. To ensure controlled conditions and a continuous contact between water and the rock bottom face, we use a water leaching process with an extremely low capillary number (8×10^{-9}) to remove the generated oil from the diffuser without inducing forced water flow into the sample.

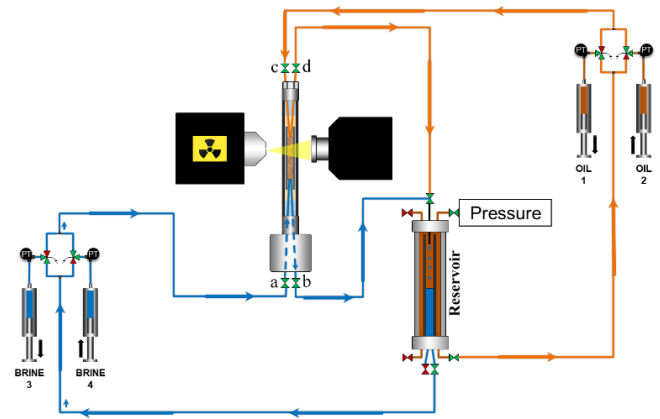


Fig 6 : Experimental set-up of the wettability anchoring experiment. In spontaneous imbibition c and d are closed, a and b are opened. In spontaneous drainage a and b are closed, c and d opened.

We perform the spontaneous imbibition process for two weeks. Then, water is injected into the sample in a forced imbibition with the same maximum capillary number used in our SCAL lab. Finally, using a similar protocol we perform a spontaneous drainage in the other face of the sample. Micro-CT acquisitions are made at the end of each phase of the experiment. At the end of this step, water relative permeability at Remaining Oil Saturation (ROS) is determined.

Subsequently, a spontaneous drainage process is conducted on the opposite face of the sample, employing a similar protocol to the spontaneous imbibition.

At the conclusion of each phase of the experiment, micro-CT acquisitions are conducted to capture detailed imaging data. This enables us to have valuable insights into the fluid behavior and distribution within the sample at different stages of the experiment.

The analysis of the images acquired before and after spontaneous imbibition reveals that there is no change in water saturation, indicating the absence of any connected water-wet clusters within the sample. Additionally, the saturation profile of the oil at ROS in displays a capillary end effect, confirming that a significant portion of the pore space is oil-wet.

During the spontaneous drainage phase, only a small volume of oil (0.05 PVs) is observed to imbibe, indicating that only a few pores with receding contact angles greater than 90 degrees are connected to the inlet.

Based on these observations, we interpret the wettability of the sample as follows:

- *Interpretation 1:* a weakly oil-wet system:
- *Interpretation 2:* a weakly oil-wet system with some water-wet pores that are disconnected
- *Interpretation 3:* a weakly oil-wet system with some strongly oil-wet pores that are predominantly disconnected

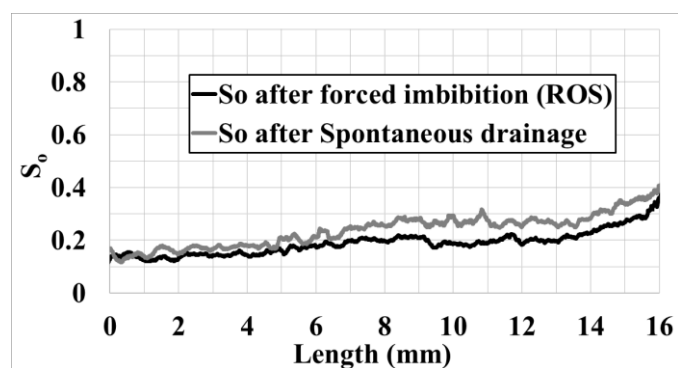


Fig 7 : Oil saturation profile at ROS (black) and after spontaneous drainage (grey)

An Amott test conducted on a sister sample, concluded a few months after the wettability anchoring experiment, exhibited no spontaneous imbibition or spontaneous drainage. This closely aligns with the results of the DRP test, further confirming the reliability and robustness of the wettability anchoring method.

This experiment also provided end point measurements that will be valuable in the simulation's selection process:

- $K_r @ ROS=0.35$
- $0.1 < S_{or} < 0.2$

5- Pore network simulations and statistical analysis

After extracting a pore network from single-phase Direct Numerical Simulation (DNS) with the associated conductance values and characterizing the wettability, we proceed to conduct two-phase flow simulations. For these simulations, we employ DynaPNM, which our inhouse pore network simulator, as described in reference [18], that we use in quasi-static mode as all the cases that we study in this paper are capillary dominated.

The pore network simulation commences by initially saturating the network with water. A primary drainage process is then simulated to establish the initial water saturation (S_{wi}). As the network is assumed to be water-wet, the injection of oil follows an invasion percolation regime. As water can escape through the wetting layers, low S_{wi} values can be achieved.

Following the primary drainage, waterflood is carried out after an aging process that alters the wettability of oil-filled pores. Initially, water spontaneously fills the water-wet portion of the network through piston-like displacement and snap-off mechanisms. During this phase, the smallest pores are filled first, followed by progressively larger ones. The defending oil phase can escape by flowing through oil-filled pores. Upon the conclusion of spontaneous imbibition, negative capillary pressure is applied to overpressure the invading water, initiating the filling of the largest pore elements first. This allows the oil to escape through the outlet via the center of oil-filled pores or oil films. The simulation continues until all the oil is trapped within the network.

The simulator has been parallelized enabling the simulation on large networks comprising tens of millions of elements can be simulated within a few hours as described in [7].

Despite conducting a wettability anchoring experiment, there remains a significant uncertainty in the input parameters. To address this, we developed a statistical uncertainty workflow [6] to incorporate this information. Within this workflow, we varied the uncertain parameters of the pore network simulation within ranges determined from the anchoring experiment. While the experiment did not directly provide information about contact angles, the observed capillary end effect indicating oil wetness and the limited oil imbibition during spontaneous drainage suggest that a considerable number of the oil-wet pores have receding contact angles below 90° . Thus, we selected medium to low oil-wet contact angles to align with this observation. Based on this, we interpreted the wettability distribution in three possible interpretations mentioned in the previous section.

Using the parameters specified in Table 1, we generated a thousand input files for DynaPNM simulations using the WSP method [18] to honor interpretations 1 and 2. Additionally, parameters from Table 2 were used to generate five hundred realizations to honor interpretation 3. No wettability correlations to the radius or in space were observed in the anchoring experiment therefore wettability has been distributed randomly in the networks.

These generated files were then used to run flow simulations on a supercomputer. A selection process was performed to retain only those realizations that aligned with the observed S_{or} (residual oil saturation) and K_{rw} (relative permeability of water) obtained from the wettability anchoring experiment.

Following the selection exercise, a simulation ranking procedure was implemented based on the oil production achieved after a specified amount of water injection corresponding to each relative permeability curve. This ranking process allowed us to define three scenarios:

- P10: an optimistic scenario in which only 10% of the simulations produce more than this case
- P50: a median scenario in which 50% of simulations produce more than this case
- P90: a pessimistic scenario in which 90% of the simulations produce more than this case

Finally, the generated DRP relative permeability curves were Corey fitted to facilitate their use in Reservoir simulations (Fig 8). As the first part of the curves is dominated by the layer flow, we focus the Corey fitting after the water breakthrough.

Table 1 : Simulation parameters used to account for wettability interpretation 1 and 2. 1000 realizations were performed.

Parameters	Value/Range
PD receding contact angle distribution	Normal distribution
PD receding contact angle standard deviation	$3^\circ-6^\circ$
Mean receding PD distribution	$20^\circ-30^\circ$

WF dist1 (oil-wet) advancing contact angle distribution	Normal distribution
WF dist1 (oil-wet), advancing contact angle standard deviation	4°-8°
Mean advancing WF dist1 (oil-wet) contact angle	100°-130°
WF dist 2 (water-wet) advancing contact angle distribution	Normal distribution
WF dist2 (water-wet), advancing contact angle standard deviation	4°- 8°
Mean advancing WF dist2 (water-wet) contact angle	60°-89°
Fraction of distribution 2 (water-wet fraction)	0.0-0.2
Correlation length	0
Wettability model	Fractional wet
Initial water saturation	0.19

Table 2 : Simulation parameters used in to account for wettability interpretation 3. 500 realizations performed using these parameters.

Parameters	Value/Range
PD receding contact angle distribution	Normal distribution
PD receding contact angle standard deviation	3°-6°
Mean receding PD distribution	20°-30°
WF dist1 (oil-wet) advancing contact angle distribution	Normal distribution
WF dist1 (oil-wet), advancing contact angle standard deviation	4°-8°
Mean advancing WF dist1 (oil-wet) contact angle	130°
WF dist 2 (water-wet) advancing contact angle distribution	Normal distribution
WF dist2 (water-wet), advancing contact angle standard deviation	20°- 30°
Mean advancing WF dist2 (water-wet) contact angle	60°-89°
Fraction of distribution 2 (water-wet fraction)	0.0
Correlation length	0
Wettability model	Fractional wet
Initial water saturation	0.19

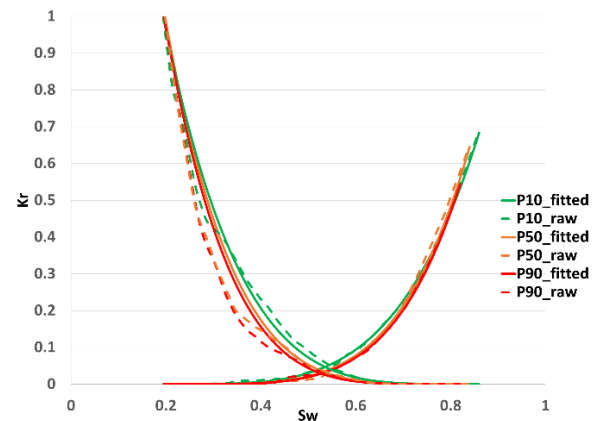


Fig 8 : Simulated and ranked relative permeability curves (at 1PV injected). P10 (Green) represents an optimistic scenario, P50 (orange) represents a median scenario and P90 (red) represents a pessimistic scenario. Dashed lines represent raw curves and continue lines represent the Corey fitted curves.

6 Comparison to SCAL experiment

After performing the blind simulation test, the numerical results are compared with those obtained during an unsteady-state experiment performed in-house.

The SCAL experiment was performed on a large Reservoir rock C core of 5 cm diameter and 20 cm length. This full-size core had a porosity of 22% with an absolute brine permeability of 328 mD. Primary drainage was achieved through viscous oil displacement, up to a targeted low S_{wi} value, with minimized capillary end-effect. A homogeneous S_{wi} profile was obtained, corresponding to an equivalent average saturation S_w of 19%. The same dead oil used on the anchoring wettability experiment was used to replace the mineral oil (with intermediate toluene replacement to avoid any asphaltene precipitation) and perform 30 days of dynamic ageing at 80°C to alter wettability of the SCAL full size plug. Afterwards, multi-rates waterflood at 80°C was performed. Initial flow rates were sized to fit Hagoort criteria [19] to avoid viscous fingering. It started at around 0.3ft/day. Oil production-pressure gradient vs time, and transient to equilibrium saturation profiles through 2D X-ray imaging in-house devices were acquired during the experiment, and the numerical interpretation was performed using the 1D core analysis software called CYDAR® to history-match oil production, pressure gradient and saturation profiles (transient and equilibrium) and to finally determine a representative couple of K_r and P_c .

Fig 9 and **Fig 10** depict our simulated relative permeability curves, incorporating the P10, P50, and P90 scenarios derived from ranking oil production after injecting one pore volume. To account for uncertainties in the inversion of experimental data, the SCAL data was represented by two realizations.

We would like to highlight that in unsteady-state relative permeability measurements, the comparison only makes sense after breakthrough (achieved at water saturation of 59.5%) and before ROS (achieved at water saturation of 73%). In this range of saturations the DRP agreed well with SCAL data. This good level of agreement instills confidence

in the predictive capabilities of DRP simulation when supported by anchoring experimental data. To further validate the simulated relative permeability curves, we compare the fractional flow curves obtained from the simulation with the SCAL experiment. **Fig 11** illustrates this comparison, demonstrating good agreement as the simulated fractional flow curves lie between the experimental curves. Additionally, we analyze the ratio of relative permeability between the simulations and experiments. **Fig 12** presents the results, indicating a strong agreement between the simulated and experimental data.

To evaluate the recovery factors associated with the experimental and DRP curves, we employ the Buckley Leverett approach. **Fig 13** showcases the recovery factors, revealing close agreement between the experimental and DRP data. These findings further reinforce the robustness of our approach. With confidence in our methodology established, we proceed to apply it to a new sample from different facies, assuming consistent wettability between the two samples.

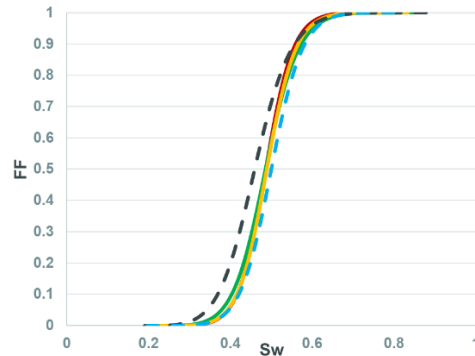


Fig 11 : Comparison between the fractional flow curves obtained from simulated Krs : P10 (green), P50 (yellow) and P90 (red) and from the experimental Krs (dashed blue and black).

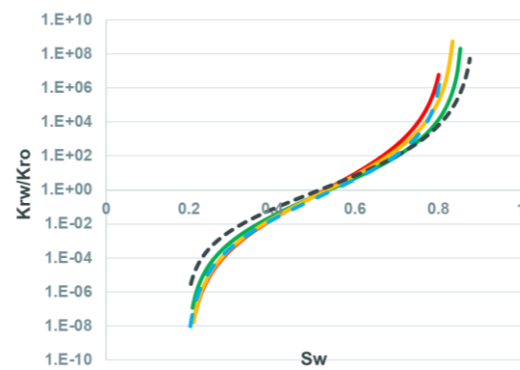


Fig 12 Comparison between the simulated ratio of relative permeability curves: P10 (green), P50 (yellow) and P90 (red) and experimental data (dashed blue and black).

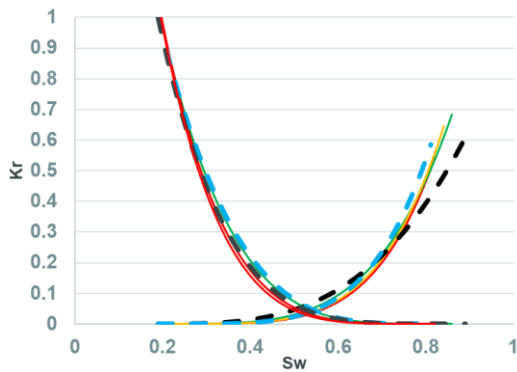


Fig 9 : Comparison between the simulated relative permeability curves: P10 (green), P50 (yellow) and P90 (red) and experimental data (dashed blue and black). We present the plots in linear scale

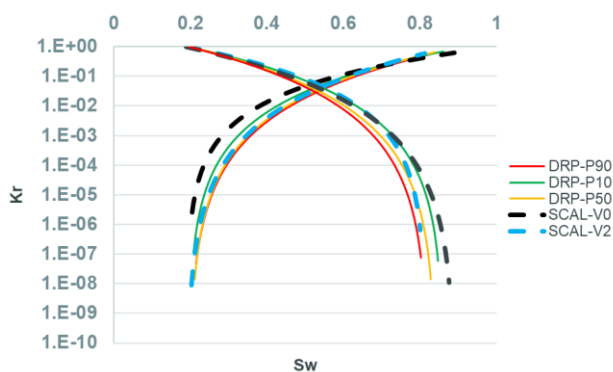


Fig 10 : Comparison between the simulated relative permeability curves: P10 (green), P50 (yellow) and P90 (red) and experimental data (dashed blue and black). We present the plots in log scale

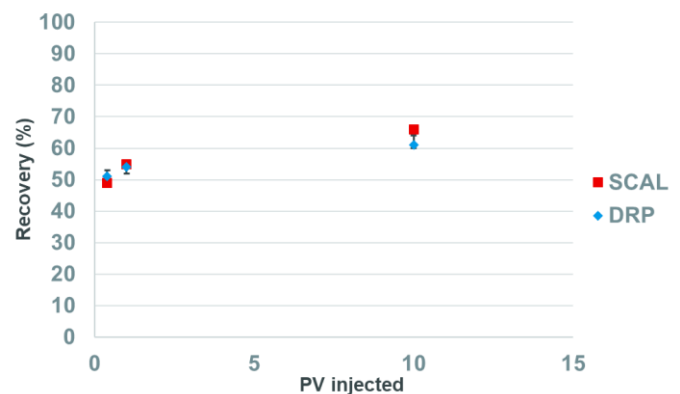


Fig 13 : Comparison between the recovery factors obtained using DRP simulated relative permeability curves (blue) and the SCAL measured relative permeability curves (red)

7 Simulations on new facies

Although performing a wettability anchoring simulation is interesting as it cuts the time of computing relative permeability by a factor 2 comparing to SCAL, there a potential to accelerate even further these measurements. If a

first wettability anchoring experiment is performed, then, assuming that wettability remains the same on other facies of the Reservoir, generating new relative permeability curves can be done in less than 2 weeks which is 12 times faster than SCAL. In order to assess the robustness of this approach, a DRP simulation study was performed on a new facies from Reservoir Rock C without repeating the wettability anchoring experiment. As same wettability was assumed, the input of the previously selected realisations (previous section) were used, then ranked to obtain P10, P50 and P90 scenarios as shown in Fig 14 and Fig 15.

A second SCAL experiment was performed on a sample from the new facies. The experiment was performed on a large Reservoir rock C core of 5 cm diameter and 20 cm length. This full -size core had a porosity of 23.3% with an absolute brine permeability of 299 mD.

It is important to emphasize that in unsteady-state relative permeability measurements, measured data are only obtained after breakthrough (occurring at a water saturation of 57.4%) and before ROS (reached at a water saturation of 73.3%). The remaining part of the Kr curve is only an extrapolation of these measured data. Within this saturation range, the DRP simulation data aligned well with the SCAL data, demonstrating a high level of agreement.

To further validate the accuracy of the simulated relative permeability curves, we conducted a comparison of the fractional flow curves obtained from the simulation and the SCAL experiment. Fig 16 visually represents this comparison, illustrating a favorable agreement as the simulated fractional flow curves fall within the range of the experimental curves. Furthermore, we performed an analysis of the relative permeability ratio between the simulations and experiments. The results, presented in Fig 17, reveal a strong agreement between the simulated and experimental data. This serves as an additional confirmation of the reliability and accuracy of the simulated relative permeability curves.

These results gave us confidence about the methodology for this Reservoir, however, it is difficult to generalize the validity of this approach for other systems with a single test especially if the wettability is correlated to pore sizes.

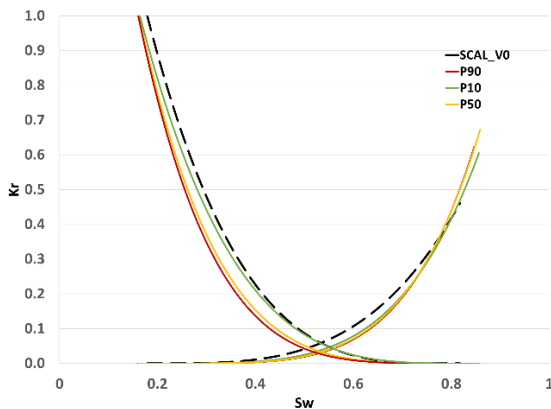


Fig 14 : Comparison between the simulated relative permeability curves: P10 (green), P50 (yellow) and P90 (red) and experimental data (dashed blue and black). We present the plots in linear scale

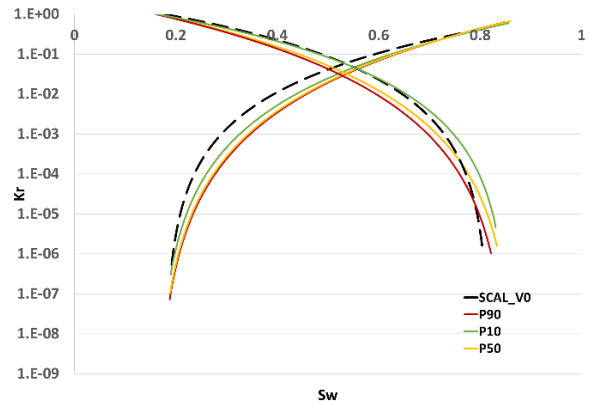


Fig 15 : Comparison between the simulated relative permeability curves: P10 (green), P50 (yellow) and P90 (red) and experimental data (dashed blue and black). We present the plots in log scale

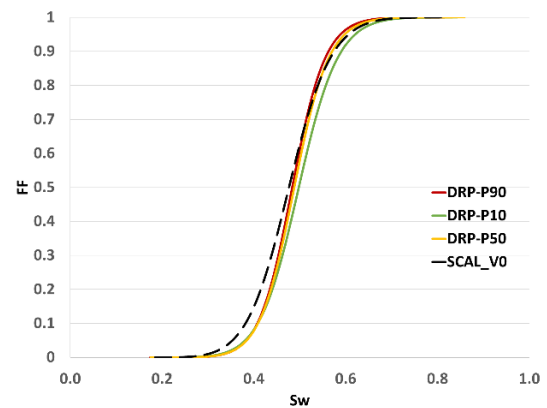


Fig 16 : Comparison between the fractional flow curves obtained from simulated Krs : P10 (green), P50 (yellow) and P90 (red) and from the experimental Krs (dashed blue and black).

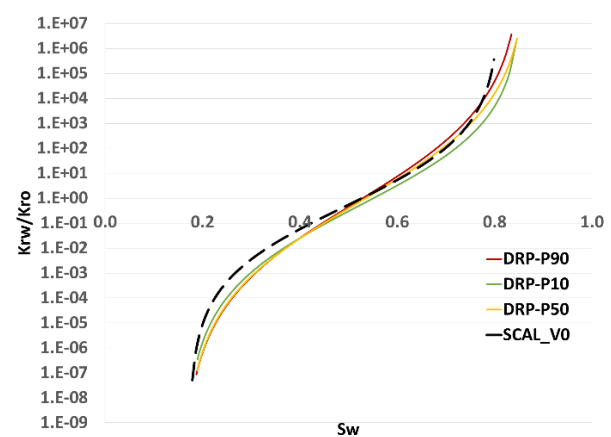


Fig 17 : Comparison between the simulated ratio of relative permeability curves: P10 (green), P50 (yellow) and P90 (red) and experimental data (dashed blue and black).

8- Conclusions

In this study, we have applied TotalEnergies' DRP workflow in an operational context. First, a DRP wettability anchoring experiment was performed to assess the wettability of the sample. This experiment provided wettability characterization consistent with the Amott Harvey test performed on a sister core. DRP accelerated this characterization by a factor 4. Furthermore, a simulation study was performed to compute relative permeability. This simulation study was informed by the anchoring experiment to provide the wettability input of the PNM simulator. This approach provided us with relative permeability data in agreement with SCAL experiment performed later. DRP coupled with wettability anchoring experiment was twice as fast as the SCAL. Finally, assuming that wettability does not change in this Reservoir, a simulation study was performed on a new facies using the same wettability parameters as the first test. This simulation study was 12 times faster than a SCAL experiment performed on a sister sample and good agreement was found between DRP simulations and SCAL during a blind test. However, more tests are needed to have a better understanding of the domain of validity of the constant wettability hypothesis especially for rocks with wettability correlated to the size of the pores.

This study was another example of the robustness of our Digital Rock Physics workflow for the prediction of relative permeability and to characterize the wettability of a sample. This approach accelerates the petrophysical synthesis and helps to develop oil and gas fields faster.

Acknowledgements

The authors would like to thank TotalEnergies management for the authorization to publish this work. ICE platform is acknowledged for acquiring the images used in this study.

Quentin DANIELCZICK is acknowledged for providing Amott Harvey data

References

- [1] Regaieg M, Nono F, Farhana Faisal, Titly, Rivenq Richard. Large Pore Network simulations coupled with innovative wettability anchoring experiment to predict relative permeability of a mixed-wet rock. (submitted). *Transport in Porous Media*, 2022.
- [2] Saxena N, Hofmann R, Alpak FO, Dietderich J, Hunter S, Day-Stirrat RJ. Effect of image segmentation & voxel size on micro-CT computed effective transport & elastic properties. *Marine and Petroleum Geology* 2017;86:972–90.
- [3] Sorbie KS, Skauge A. Can Network Modeling Predict Two-Phase Flow Functions? *SPWLA-2012-v53n6a2* 2012;53(06):401–9.
- [4] Bondino I, Hamon G, Kallel W, Kac D. Relative Permeabilities From Simulation in 3D Rock Models and Equivalent Pore Networks: Critical Review and Way Forward1. *SPWLA-2012-v53n6a2* 2013;54(06):538–46.
- [5] Regaieg M, Varloteaux C, Farhana Faisal T, ELAbid Z. Towards Large-Scale DRP Simulations: Generation of Large Super-Resolution images and Extraction of Large Pore Network Models. *Transport in Porous Media* 2023;147(2):375–99.
- [6] Regaieg M, Bondino I, Varloteaux C, Farhana Faisal T, Yang J, Rivenq R (editors). Large two phase Digital Rock Physics simulations for relative permeability uncertainty assessment; 2021.
- [7] Regaieg M, Nono F, Faisal TF, Rivenq R. Large-Pore Network Simulations Coupled with Innovative Wettability Anchoring Experiment to Predict Relative Permeability of a Mixed-Wet Rock. *Transport in Porous Media* 2023;147(2):495–517.
- [8] AlRatrouf A, Raeini AQ, Bijeljic B, Blunt MJ. Automatic measurement of contact angle in pore-space images. *Advances in Water Resources* 2017;109:158–69.
- [9] Sun C, McClure JE, Mostaghimi P, Herring AL, Meisenheimer DE, Wildenschild D, Berg S, Armstrong RT. Characterization of wetting using topological principles. *J Colloid Interface Sci* 2020;578:106–15.
- [10] Foroughi S, Bijeljic B, Lin Q, Raeini AQ, Blunt MJ. Pore-by-pore modeling, analysis, and prediction of two-phase flow in mixed-wet rocks. *Phys. Rev. E* 2020;102(2):23302.
- [11] AlRatrouf A, Blunt MJ, Bijeljic B. Spatial Correlation of Contact Angle and Curvature in Pore-Space Images. *Water Resour. Res.* 2018;54(9):6133–52.
- [12] Raeini AQ, Bijeljic B, Blunt MJ. Generalized network modeling: Network extraction as a coarse-scale discretization of the void space of porous media. *Phys. Rev. E* 2017;96(1):13312.
- [13] Yang J, Bondino I, Regaieg M, Moncorgé A. Pore to pore validation of pore network modelling against micromodel experiment results. *Computational Geosciences* 2017;21(5):849–62.
- [14] Wang X, Yu K, Wu S, Gu J, Liu Y, Dong C, Qiao Y, Change Loy C. Esrgan: Enhanced super-resolution generative adversarial networks. In: *Proceedings of the European conference on computer vision (ECCV) workshops*. p. 0.
- [15] Arganda-Carreras I, Kaynig V, Rueden C, Eliceiri KW, Schindelin J, Cardona A, Sebastian Seung H. Trainable Weka Segmentation: a machine learning tool for microscopy pixel classification. *Bioinformatics* 2017;33(15):2424–6.

- [16] Berg S, Saxena N, Shaik M, Pradhan C. Generation of ground truth images to validate micro-CT image-processing pipelines. *The Leading Edge* 2018;37(6):412–20.
- [17] Reinhardt M, Jacob A, Sadeghnejad S, Cappuccio F, Arnold P, Frank S, Enzmann F, Kersten M. Benchmarking conventional and machine learning segmentation techniques for digital rock physics analysis of fractured rocks. *Environmental Earth Sciences* 2022;81(3):71.
- [18] Regaieg M, Moncorgé A. Adaptive dynamic/quasi-static pore network model for efficient multiphase flow simulation. *Computational Geosciences* 2017;21(4):795–806.
- [19] Hagoot J. Displacement stability of water drives in water-wet connate-water-bearing reservoirs. *Society of Petroleum Engineers Journal* 1974;14(01):63–74.